Threshold Modeling of Autonomic Control of Heart Rate Variability

Garrett B. Stanley*, *Associate Member, IEEE*, Kameshwar Poolla, *Member, IEEE*, and Ronald A. Siegel

***Abstract*—Even in the absence of external perturbation to the human cardiovascular system, measures of cardiac function, such as heart rate, vary with time in normal physiology. The primary source of the variation is constant regulation by a complex control system which modulates cardiac function through the autonomic nervous system. Here, we present methods of characterizing the statistical properties of the underlying processes that result in variations in ECG R-wave event times within the framework of an integrate-and-fire model. We first present techniques for characterizing the noise processes that result in heart rate variability even in the absence of autonomic input. A relationship is derived that relates the spectrum of R–R intervals to the spectrum of the underlying noise process. We then develop a technique for the characterization of the dynamic nature of autonomically related variability resulting from exogenous inputs, such as respiratory-related modulation. A method is presented for the estimation of the transfer function that relates the respiratory-related input to the variations in R-wave event times. The result is a very direct analysis of autonomic control of heart rate variability through noninvasive measures, which provides a method for assessing autonomic function in normal and pathological states.**

***Index Terms*—Autonomic nervous system, heart rate variability, stochastic processes, threshold models.**

I. Introduction

In HEALTHY humans, the sino-atrial (SA) node acts as the pacemaker for the heart. Through an upward drift in electrical potential, these cells spontaneously depolarize to a threshold potential, at which point they rapidly depolarize, or "fire" as a group. This event is followed by a reset which marks the start of a new cycle. Firing initiates the spread of electrical activity throughout the heart, followed by contraction of cardiac muscle. The R-wave of an electrocardiogram (ECG), which is readily localized in time, provides a convenient marker from which periods between SA node firings can be gleaned.

The spontaneous depolarization of SA nodal cells has an intrinsic rate that is regulated by direct input from the sympathetic and parasympathetic branches of the autonomic nervous system (ANS). Neural impulses arriving from the sympathetic branch tend to increase the mean HR, while impulses from the parasympathetic branch have the opposite effect. By this means, the ANS regulates HR.

Generally speaking, neural impulses do not occur with exact regularity. Rather, they exhibit random variation around a mean rate. As a result, not only the mean rate of SA node firing is affected by ANS input, but the beat-to-beat intervals measured from the ECG also have a stochastic component, which may be termed "heart rate variability" (HRV) [1]. Interestingly, normal individuals show much greater HRV than those whose ANS function is attenuated due to aging, disease states, or pharmacologic blockade [2]–[5]. It has been found that HRV, while random, exhibits a correlation structure in time, which can be associated with various periodicities of modulation of HR. Activity of the higher respiratory centers has been shown to modulate HR at the respiratory frequency via the parasympathetic branch of the ANS [3], [6]–[8]. Also, the baroreflex feedback mechanism modulates HR through both branches of the ANS at sub-respiratory frequencies [2], [3], [9], [10].

In this paper, we present a sequence of models of heart rate which take into account the spontaneous activity of the SA pacemaker, as well as the presence of autonomic inputs. These models are variants of integrate and fire, or integral pulse frequency modulation (IPFM) models which have been introduced previously [11], [12]. In our models, constant inputs to an integrate-and-fire mechanism are supplemented by stochastic inputs which are intended to represent disturbances due to intrinsic pacemaker fluctuations and respiratory inputs. Relationships between the stochastic properties of these disturbances and characteristics of observed HR time series are derived, and examples of the utility of this modeling scheme are presented.

II. A Noise Model

Consider first a simple threshold model where the inputs to an integrator are a constant, β, and Gaussian white noise process, $\boldsymbol{e}$, with zero mean and variance σ_e^2 (all random variables will be denoted with boldface). This corresponds to the situation where autonomic input is removed and the heart continues to "beat," yet there is some residual amount of variation in the inter-event intervals that we will attribute to "noise."

The output of the integrator, $\boldsymbol{y}$, is compared to a fixed threshold, and upon reaching the threshold, an event occurs and the integrator is reset to zero. A block diagram of the mechanism is shown in Fig. 1. Prior to the first time crossing of threshold, we can represent this system in the following form:

$$\boldsymbol{y}(t) = \int_0^t [\beta + \boldsymbol{e}(\lambda)]\, d\lambda \tag{1}$$

Manuscript received May 25, 1999; revised March 10, 2000. This work was performed during the tenure of a research Fellowship from the American Heart Association, California Affiliate, and was supported in part by National Institute of Health (NIH) under Grant GM-26691. *Asterisk indicates corresponding author*.

*G. B. Stanley is with the Division of Engineering and Applied Sciences, Harvard University, 29 Oxford Street, Cambridge, MA 02138 USA (e-mail: gstanley@deas.harvard.edu).

K. Poolla is with the Departments of Mechanical and Electrical Engineering, University of California, Berkeley, CA 94720 USA.

R. A. Siegel is with the Departments of Pharmaceutics and Biomedical Engineering, University of Minnesota, Minneapolis, MN 55455 USA.

Publisher Item Identifier S 0018-9294(00)08001-0.

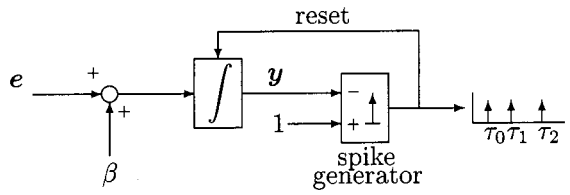

Fig. 1. Threshold noise model.

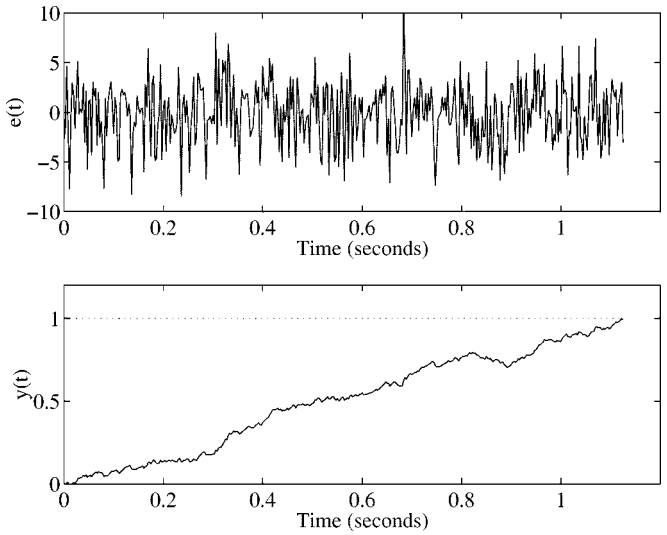

Fig. 2. (top) Gaussian white noise process and (bottom) corresponding potential increasing to threshold. The amount of noise has been exaggerated for demonstration.

We are interested in the time $\boldsymbol{T}$ at which the threshold level is crossed by $\boldsymbol{y}$, as shown in Fig. 2. Equation (1) can be expressed as

$$\boldsymbol{y}(t) = \beta t + \boldsymbol{w}(t). \tag{2}$$

The term $\boldsymbol{w}(t)$ is an integrated white noise process over the interval from zero to t. The process $\boldsymbol{w}(t)$ is, therefore, a Wiener process, which is known to have a Normal distribution $\mathcal{N}(0, \sigma_e^2 t)$. The process $\boldsymbol{y}(t)$ is, therefore, distributed as $\mathcal{N}(\beta t, \sigma_e^2 t)$.

We are interested in the first passage time $\boldsymbol{T}$ at which $\boldsymbol{y}$ first crosses 1, since firing and reset occur at this time. The first passage time is known to have the density [13]

$$f_T(T) = \frac{1}{\sqrt{2\pi\sigma_e^2 T^3}} \exp\left\{ -\frac{\left(T - \frac{1}{\beta}\right)^2}{\frac{2T\sigma_e^2}{\beta^2}} \right\}. \tag{3}$$

For $\beta > 10\sigma_e$ (see Fig. 3), this density is very well approximated by

$$f_{\boldsymbol{T}}(T) \approx \frac{1}{\sqrt{2\pi\frac{\sigma_e^2}{\beta^3}}} \exp\left\{ -\frac{\left(T - \frac{1}{\beta}\right)^2}{2\frac{\sigma_e^2}{\beta^3}} \right\} \tag{4}$$

which is $\mathcal{N}((1/\beta), (\sigma_e^2/\beta^3))$.

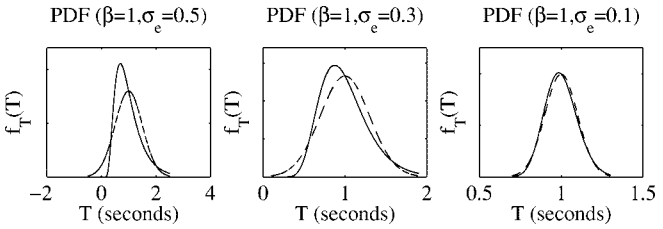

Fig. 3. Actual (solid) and approximate (dashed) probability density functions for a range of β to σ_e ratios.

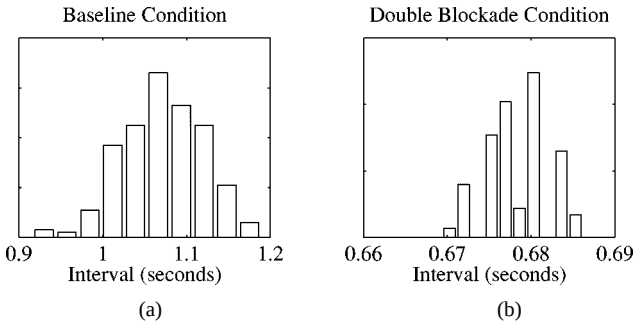

Fig. 4. Interval histograms (a) before (mean = 1.07, $\sigma = 0.048$) and (b) after (mean = 0.679, $\sigma = 0.0037$) double pharmacological autonomic blockade [8].

Consider now a set of R–R intervals $T_1, T_2, \ldots, T_n$, measured in the absence of autonomic input (i.e. after double pharmacological autonomic blockade). Assuming the data are generated from a system of the structure shown in Fig. 1, the probability density function of the intervals between heart beats can be related to that of the noise, $\boldsymbol{e}(t)$. For this model, β and σ_e^2 are the only parameters necessary to completely describe the system. For the prescribed threshold of one, β can immediately be estimated as the reciprocal of the mean interval length, $\hat{\mu}_T$, and is representative of the intrinsic firing rate of the SA node in the absence of autonomic input. The sequence of intervals will be independent and identically distributed (IID), each interval distributed as prescribed in (4). The variance of the hidden noise process, σ_e^2, can be estimated from the estimated variance of the sequence of intervals, $\hat{\sigma}_T^2$:

$$\begin{aligned} \hat{\sigma}_e^2 &= \hat{\beta}^3 \hat{\sigma}_T^2 \\ &= \frac{1}{\hat{\mu}_T^3} \hat{\sigma}_T^2. \end{aligned} \tag{5}$$

Fig. 4 shows typical interval histograms for the baseline condition and for the case when effects of the autonomic nervous system have essentially been removed through double pharmacological blockade. Data shown are real data collected during a previous study by our group [7]. For both cases, the modulation about the mean interval length is small relative to the mean interval length and the interval histogram appears to be Gaussian.

III. A More General Class of Noise Models

One underlying assumption above is the whiteness of the additive noise in the threshold model. Let us evaluate this assumption for an experimentally observed sequence of intervals between R-waves under double pharmacological autonomic blockade, where the inputs from both branches of the autonomic nervous system are presumably suppressed [14].

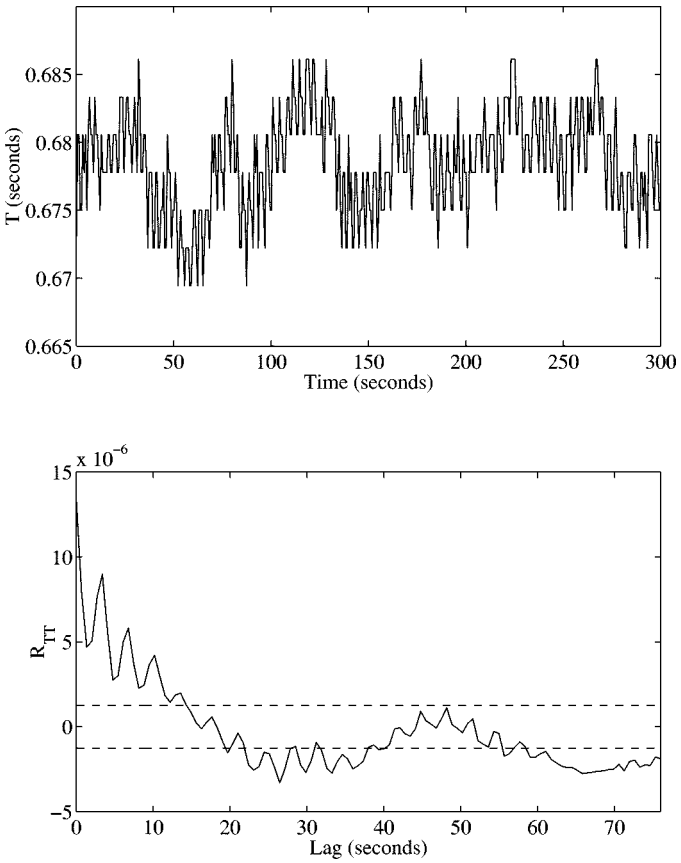

Fig. 5. Experimentally observed (top) sequence of intervals and (bottom) autocovariance of intervals after pharmacological block of the autonomic nervous system input. Note that the data presented were collected during a previously published study [7].

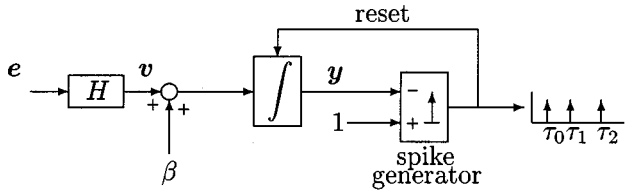

Fig. 6. General threshold noise model

In this case, the intervals reveal the nature of the process noise, suggesting some type of time-dependent correlation, however, that cannot be accounted for by the previous model. Results from a previous study, shown in Fig. 5, reveal the nature of the time-dependent correlation [7]. The bottom panel of Fig. 5 shows the autocovariance of the experimentally observed interspike intervals, R_{TT}, assuming that the process is stationary. Dashed lines represent the 95% confidence interval on a white process. It is obvious from this figure that the noise process is not white. It should be noted that the higher frequency fluctuations that are apparent in the autocovariance estimate are related to respiration. It is unclear whether this respiratory influence is due to incomplete blockade of autonomics or due to mechanical coupling, as has been suggested previously [2].

To account for the inter-interval correlation structure consider the more general threshold model shown in Fig. 6, where the process noise is modeled as filtered white noise, the filter being denoted by H. Consider the threshold crossing times $\boldsymbol{\tau}_0, \boldsymbol{\tau}_1, \ldots$, and define the interspike interval as $\boldsymbol{T}_k = \boldsymbol{\tau}_k - \boldsymbol{\tau}_{k-1}$. Again setting the threshold level to one, we write the following equation for a threshold model in which the input to the integrator is the sum of a filtered white noise process and a constant β

$$\begin{aligned}\int_{\boldsymbol{\tau}_{k-1}}^{\boldsymbol{\tau}_k} [\boldsymbol{v}(\lambda)+\beta]\,d\lambda &= 1\\ \int_{\boldsymbol{\tau}_{k-1}}^{\boldsymbol{\tau}_k} \boldsymbol{v}(\lambda)\,d\lambda + \beta\boldsymbol{T}_k &= 1\\ \boldsymbol{q}_k + \beta\boldsymbol{T}_k &= 1 \end{aligned} \tag{6}$$

where $\boldsymbol{v}(t) = h(t) * \boldsymbol{e}(t)$, $\boldsymbol{q}_k$ is the integrated colored noise process over the interval from $\boldsymbol{T}_{k-1}$ to $\boldsymbol{T}_k$, $h(t)$ is the impulse response of the filter H, and $\boldsymbol{e}(t)$ is Gaussian white noise $\sim \mathcal{N}(0, 1)$. Equation (6) can be written as

$$\int_0^{\boldsymbol{T}_k} \boldsymbol{v}(\lambda+\boldsymbol{\tau}_{k-1})\,d\lambda + \beta\boldsymbol{T}_k = 1$$

which, assuming small variations of the interspike intervals around the mean, can be approximated by

$$\int_0^{\mu_T} \boldsymbol{v}(\lambda+(k-1)\mu_T)\,d\lambda + \beta\boldsymbol{T}_k \approx 1. \tag{7}$$

The expectation of the integrated noise can be calculated

$$\begin{aligned} E\{\boldsymbol{q}_k\} &\approx E\{1-\beta\boldsymbol{T}_k\}\\ &= 1-\beta\mu_T. \end{aligned} \tag{8}$$

Since $\boldsymbol{v}$ is the output of a linear system with zero mean input, $\boldsymbol{q}$ will also have mean approximately zero, implying again that $\mu_T \approx (1/\beta)$.

We can then determine the autocovariance of the integrated noise $\boldsymbol{q}$

$$\begin{aligned} R_{qq}[p\mu_T] &= E\{\boldsymbol{q}_k\boldsymbol{q}_{k+p}\}\\ &= E\{[1-\beta\boldsymbol{T}_k][1-\beta\boldsymbol{T}_{k+p}]\}\\ &= \beta^2 R_{TT}[p\mu_T] \end{aligned} \tag{9}$$

where $p = 0, 1, 2, \ldots$ Note that the autocovariance function is evaluated at multiples of the mean interval length, μ_T. This relationship can be expanded further

$$\begin{aligned} &R_{TT}[p\mu_T]\\ &\quad= \frac{1}{\beta^2}R_{qq}[p\mu_T]\\ &\quad= \frac{1}{\beta^2}E\left\{\int_{\boldsymbol{\tau}_{k-1}}^{\boldsymbol{\tau}_k}\int_{\boldsymbol{\tau}_{k+p-1}}^{\boldsymbol{\tau}_{k+p}} \boldsymbol{v}(\lambda)\boldsymbol{v}(\gamma)\,d\lambda\,d\gamma\right\}\\ &\quad= \frac{1}{\beta^2}E\left\{\int_0^{\boldsymbol{T}_k}\int_0^{\boldsymbol{T}_{k+p}} \boldsymbol{v}(\lambda+\boldsymbol{\tau}_{k-1})\times\boldsymbol{v}(\gamma+\boldsymbol{\tau}_{k+p-1})\,d\lambda\,d\gamma\right\}. \end{aligned}$$

If the variations of the inter-spike intervals around the mean are small, then the following approximation can be made:

$$R_{TT}[p\mu_T] \approx \mu_T^2 E\left\{\int_0^{\mu_T}\int_0^{\mu_T} \boldsymbol{v}(\lambda+(k-1)\mu_T) \times \boldsymbol{v}(\gamma+(k+p-1)\mu_T)\,d\lambda\,d\gamma\right\} = \mu_T^2\int_0^{\mu_T}\int_0^{\mu_T} R_{vv}(\gamma-\lambda+p\mu_T)\,d\lambda\,d\gamma.$$

Defining a function $\Pi_{\mu_T}(t)$ that equals one on $t \in [0,\ \mu_T]$ and zero elsewhere, we can write the following:

$$R_{TT}[p\mu_T] \approx \mu_T^2\int_{-\infty}^{\infty}\int_{-\infty}^{\infty} R_{vv}(\gamma-\lambda+p\mu_T) \times \Pi_{\mu_T}(\lambda)\Pi_{\mu_T}(\gamma)\,d\lambda\,d\gamma = \mu_T^2 R_{vv}[p\mu_T] * \Pi_{\mu_T}[p\mu_T] * \Pi_{-\mu_T}[p\mu_T].$$

Now $\Lambda(t) := \Pi_{\mu_T}(t) * \Pi_{-\mu_T}(t)$ is a triangle wave that equals $\mu_T - |t|$ for $|t| \le \mu_T$, and zero, otherwise. This triangle wave is so narrow relative to the time scale of R_{TT} that it is well approximated by a discrete impulse $\mu_T\delta[p\mu_T]$

$$R_{TT}[p\mu_T] \approx \mu_T^3 R_{vv}[p\mu_T]. \tag{10}$$

Note that the expression in (10) is a more general case of the relationship between the second-order statistics of the intervals and the noise, as compared to that developed in the white noise case. Taking the Fourier transform of both sides, we obtain a relationship between the spectrum of intervals and the noise model H

$$S_{TT}(\omega) \approx \mu_T^3 S_{vv}(\omega) = \mu_T^3|H(\omega)|^2 S_{ee}(\omega) \tag{11}$$

where the $S_{ee}(\omega)$ can be dropped since $\boldsymbol{e}$ is a white noise process and $S_{ee}(\omega)$ is constant across all frequencies. The squared modulus of the noise filter H can then be estimated directly from estimates of μ_T and S_{TT}.

As an example, let $\beta = 1.5$, and let H have the form $H(s) = (0.085s^2 + 0.28s + 0.26)/(s^2 + 4.9s + 0.59)$. We can simulate a sequence of intervals, estimate the corresponding autocovariance, and estimate the noise filter H, as shown in Fig. 7. The simulated sequence of intervals exhibits similar characteristics to those observed experimentally in Fig. 5, so this serves as a method of validation for our procedure. The relationship in (11) provides a reasonably accurate estimate of the noise filter H, as is shown in the bottom panel of Fig. 7.

There are limitations on the identification of the noise model as discussed previously in Section II. The major underlying assumption is that the noise is "small" relative to the influence of the ramp. For the noise model constructed in this section, approximations will hold provided β is large relative to $\sigma_v = ||H||\sigma_e$. As was shown in the right panel of Fig. 4, this is indeed what is observed experimentally. Other limitations of the estimation procedure stem from the finite sample length which sets a lower bound on frequency resolution (e.g. 0.01 Hz or so for a 5-min sample). One concern is the nonlinear distortions in the spectra that have been observed in previous studies by de Boer *et al.* [15]. To test the technique presented here, we simulated the response to a single oscillatory input, which resulted in a peak in the spectrum at the fundamental frequency and smaller peaks at higher harmonics. The simulated response to the superposition of two oscillatory inputs at different frequencies also resulted in similar distortions. In all cases the sideband power was nearly identical to that observed from spectra of the interspike intervals, as a result of harmonic distortion and aliasing [15].

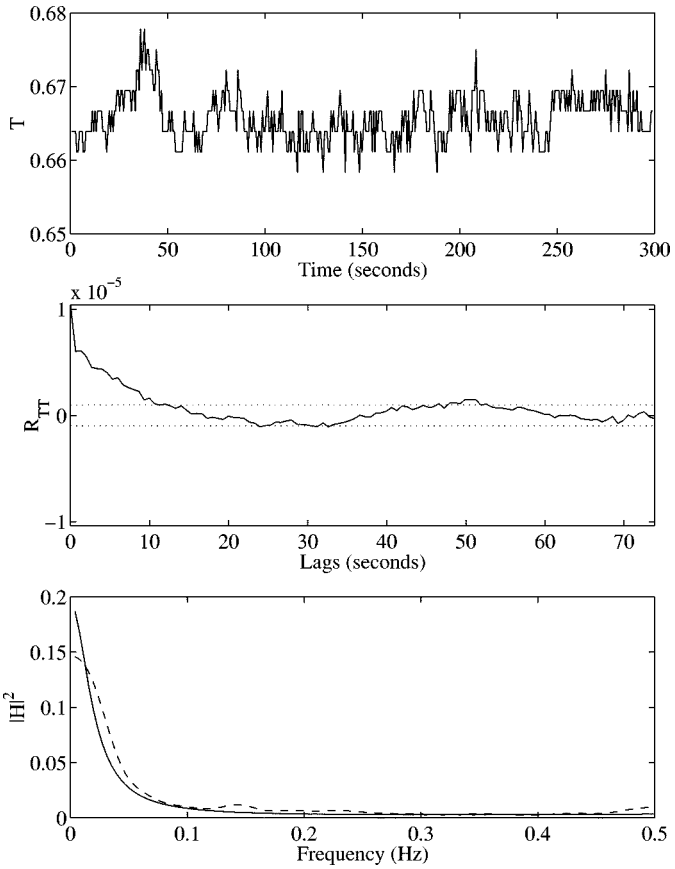

Fig. 7. (top) Simulated sequence of intervals and (middle) estimated autocovariance of the intervals R_{TT}. (bottom) Actual (solid) versus estimated (dashed) squared modulus of the noise filter.

IV. Input Driven Treshold Model

Lung volume is known to be correlated with variations in the timing of heart beats. This phenomenon is known as respiratory sinus arrhythmia (RSA). Activity of the respiratory rhythm generator has been shown to modulate the release of vagal neurotransmitter at the SA node and, therefore, modulate the rate of depolarization at the respiratory frequency [16]. In order to noninvasively characterize the activity of the respiratory rhythm generator, we measured lung volume of subjects at rest, and propose that this measurement is sufficient to represent central rhythm activity.

In order to develop models of respiratory sinus arrhythmia, we turn our attention to a general class of input driven threshold models. Consider the model shown in Fig. 8.

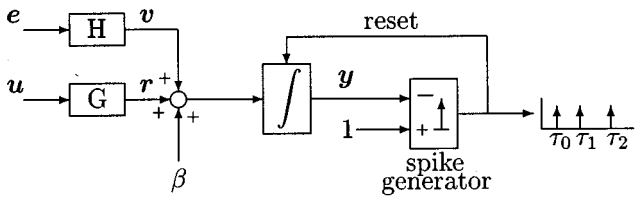

Fig. 8. Input driven threshold model

We can write the following relationship:

$$\int_{\tau_{k-1}}^{\tau_k} [\boldsymbol{v}(\lambda) + \boldsymbol{r}(\lambda) + \beta]\, d\lambda = 1$$
$$\int_{\tau_{k-1}}^{\tau_k} [\boldsymbol{v}(\lambda) + \boldsymbol{r}(\lambda)]\, d\lambda + \beta \boldsymbol{T}_k = 1$$
$$\boldsymbol{\Phi}_k + \beta \boldsymbol{T}_k = 1 \tag{12}$$

where $\boldsymbol{r}$ is a filtered version the zero-mean respiratory input $\boldsymbol{u}$, and $\boldsymbol{v}$ is the output of a filter whose input is Gaussian white noise. $\boldsymbol{\Phi}_k$ represents the sum of the noise activity and the respiratory influence, integrated over the interval from $\boldsymbol{T}_{k-1}$ to $\boldsymbol{T}_k$. We restrict input $\boldsymbol{u}$ to be zero mean and, therefore, $E\{\boldsymbol{\Phi}_k\}$ will also be zero, producing $\mu_T \approx (1/\beta)$. β in this case is representative of a combination of the intrinsic firing rate of the SA node and the mean levels of parasympathetic and sympathetic activity. We can relate the second-order statistics of $\boldsymbol{\Phi}$ to the second-order statistics of the intervals

$$R_{\Phi\Phi}[p\mu_T] = E\{\boldsymbol{\Phi}_k \boldsymbol{\Phi}_{k+p}\}$$
$$= \beta^2 R_{TT}[p\mu_T].$$

We can then make the following approximation:

$$R_{TT}[p\mu_T] = \mu_T^2 R_{\Phi\Phi}[p\mu_T]$$
$$\approx \mu_T^3 \{R_{vv}[p\mu_T] + R_{rr}[p\mu_T]\} \tag{13}$$

using independence of $\boldsymbol{v}$ and $\boldsymbol{r}$. In the frequency domain we have the relationship

$$S_{TT}(\omega) \approx \mu_T^3 \{S_{vv}(\omega) + S_{rr}(\omega)\}$$
$$= \mu_T^3 \{|H(\omega)|^2 + |G(\omega)|^2 S_{uu}(\omega)\}. \tag{14}$$

Given the observed sequence of R–R intervals, the measured respiratory input u, and the previously identified noise model obtained from the double-blockade condition, we can, therefore, estimate the respiratory-related transfer function magnitude, $|G(\omega)|$. This estimate relies on the assumption that the underlying dynamics of the noise process is unchanged through the application of double pharmacological autonomic blockade. In order to estimate the phase of G, it is necessary to reconstruct $\boldsymbol{\Phi}$ from observed intervals. From the discontinuous sequence $\boldsymbol{\Phi}$, we can then construct a continuous sequence $\boldsymbol{\Psi}$ by eliminating the discontinuities caused by the reset mechanism

$$\Psi_k = \sum_{j=1}^{k} \boldsymbol{\Phi}_j. \tag{15}$$

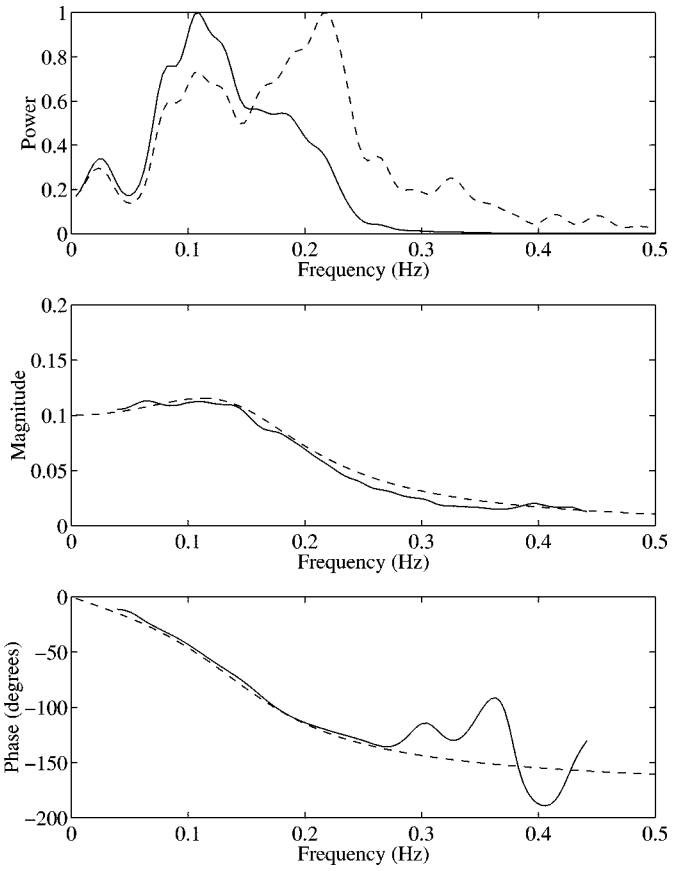

Fig. 9. (top) Lung volume (dashed) and simulated R–R interval spectrum (solid), both normalized for comparison. (middle and bottom) Estimated (solid) and actual (dashed) transfer function magnitude and phase, respectively. Note the large error at higher frequencies, attributed to insufficient input excitation in this frequency range.

From the constructed sequence, the phase can then be estimated

$$\angle G(\omega) = \angle \frac{S_{\Psi u}}{S_{uu}} + 90^\circ \tag{16}$$

where $S_{\Psi u}(\omega)$ is the cross-spectrum between the input $\boldsymbol{u}$, and the constructed signal $\boldsymbol{\Psi}$. Note that the pure integrator of the model produces a phase shift of 90°, which is accounted for in (16).

Consider data collected through broad-band respiration experiments, which we have described previously [7]. Dynamics of respiratory influence on heart rate have been shown to exhibit low-pass characteristics. Let us, therefore, assume that the input enters into the threshold model through a low-order low-pass system, $G(s) = 0.1/(s^2 + s + 1)$. Furthermore, let us assume $\beta = 1$, and that the noise model, H, is as previously identified through the use of double pharmacological autonomic blockade. To illustrate the concepts developed in this section, we can simulate a sequence of intervals, based on the model prescribed above. From the simulation, we observe the sequence $\boldsymbol{T}$ and can construct the sequence $\boldsymbol{\Phi}$. From the information about $\boldsymbol{\Phi}$ and $\boldsymbol{T}$, we can then estimate G, as we have discussed. The normalized input and output spectra, as well as the actual and estimated transfer functions are shown in Fig. 9. We see that the techniques provide excellent estimates of the input filter characteristics for

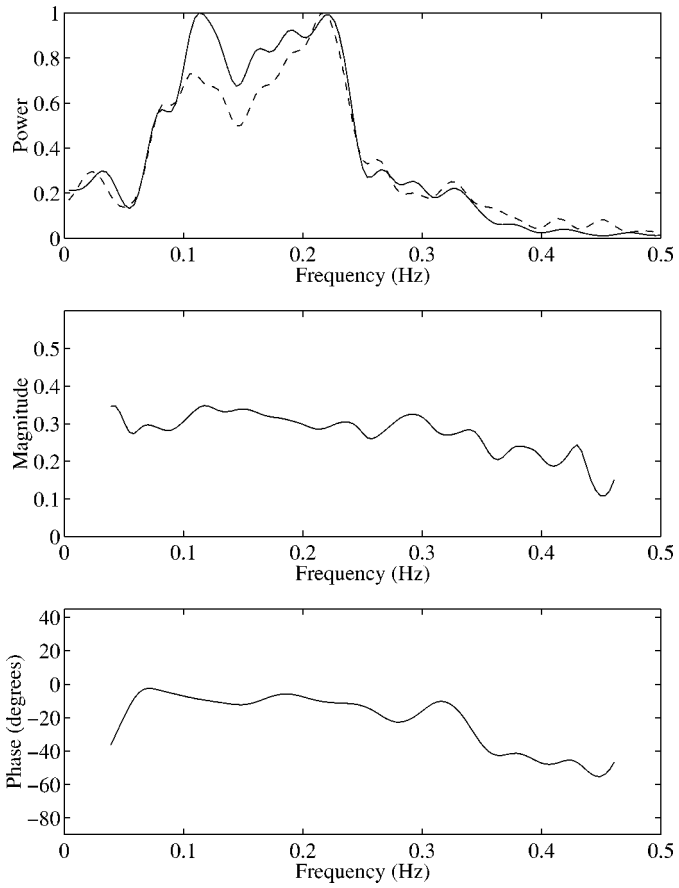

Fig. 10. (top) Interval spectrum (solid) and lung volume spectrum (dashed), both normalized for comparison. (middle and bottom) Estimated transfer function magnitude and phase, respectively.

this simulated example. The previous example serves as a validation for our technique, which can then be directly applied to experimentally observed lung volume and R-wave event times.

Fig. 10 shows the lung volume and R–R interval spectra for a typical data set from a previously published study [7], along with the corresponding transfer function magnitude and phase estimates over frequency bands of high coherence. The resulting estimate is in agreement with our previous findings [7], where it was shown that the transfer function magnitude tends to be rather flat over frequency bands of sufficient excitation. The relative phase from our previous study exhibited similar characteristics, but the absolute value of phase is less ambiguous when computed with the technique presented here.

As in Section II, we again have some limitations on our modeling procedure. The size of the modulating signals must be small relative to the ramp. Let $\boldsymbol{m} := \boldsymbol{v} + \boldsymbol{r}$. From Section III, we know that the approximations hold for β large relative to σ_m. This implies that our constraint becomes $\beta \gg \sqrt{\sigma_v^2 + \sigma_r^2} = \sqrt{||H||^2\sigma_e^2 + ||G||^2\sigma_u^2}$ since $\boldsymbol{v}$ and $\boldsymbol{r}$ are independent by assumption, where σ_u^2 is the variance of the input $\boldsymbol{u}$. Note also that the same bandwidth limitations exist in this input case as for the noise filter estimation in Section III. Also, as discussed in Section III, nonlinear distortions are present which effectively cause a certain degree of aliasing in the interval spectrum. We would, therefore, expect this distortion to affect the subsequent estimation of the transfer function, G, which could explain the slight mismatch between the actual and estimated transfer functions of the simulation shown in Fig. 9. Finally, there is autonomic modulation that is not associated with respiration, as discussed previously. This activity is typically at frequencies lower than the spontaneous respiratory frequency, allowing the estimation of the transfer function over the respiratory frequency range, as outlined above. However, for broad-band respiration, the estimate of the transfer function at low frequencies will, therefore, be biased by this nonrespiratory modulation.

V. Conclusion

In this paper, we have presented a physiologically inspired stochastic model describing heart rate variability. The underlying physiology suggests temporal and spatial integration of autonomic activity, producing variations in the rate at which the SA nodal cells depolarize to threshold and "fire." The model presented directly addresses both the basic physiological nature of the system and the somewhat less understood observed phenomena of variability through inputs to an integrate-and-fire mechanism of SA nodal activity. It was shown that in the absence of autonomic nervous system input, noise models could be estimated directly to obtain characterizations of the unmodeled dynamics of the system as well as external disturbances. The model presented characterizes the noise as fluctuations in ANS input, rather than the less direct description of "noise" in the HR output previously suggested. The intrinsic firing rate of the SA node was captured in the constant input to the threshold model in the absence of autonomic input, rather than simply as the mean of the observed heart rate. Furthermore, the effect of the ANS on mean SA nodal firing rate was captured as the difference in the constant input to the integrate-and-fire mechanism in the absence and presence of sympathetic and parasympathetic nervous system activity. It was also shown that through similar arguments, the dynamic relationship between the exogenous inputs, such as respiratory related autonomic activity, and the sequence of interspike intervals could be captured.

The commonly accepted procedure of characterizing autonomic mediation of the rate at which the heart beats through the artificial construct of "heart rate" has been used extensively in a number of applications [2]–[5]. We and others have used this construct to successfully capture autonomic mediation of heart rate at respiratory frequencies, as well as lower frequencies associated with baroreflex activity [2], [8], [7]. Although the traditional techniques essentially capture the magnitude of influence by autonomic activity, the current works presents perhaps a more straightforward approach that relates directly to the physiological mechanisms involved. Furthermore, problems often arise in the interpretation of phase relationships evaluated through the artificial construct of heart rate, but for the threshold modeling techniques presented in this work, the interpretations are clear. One limitation of this technique arises from the fact that we have presented a model based on Gaussian noise processes, whereas the underlying neural inputs are actually point events. We expect this limitation to have little effect on the predictive capability of the technique. We have also assumed that the residual noise is unaffected by the presence of blockade; this assumption was made for simplicity. Another limitation resides

in the estimation procedure, which we have shown to exhibit slight nonlinear distortions and potential biases at nonrespiratory frequencies. Finally, the analysis is essentially linear except for the introduction of the threshold mechanism. Models which assume more fundamental nonlinearities have been examined by others [17], [18], which could enhance the techniques presented here. The utility of the techniques developed in this work lies in the direct analysis of autonomic activity through physiologically based mechanisms, without the construction of intermediate characterizations of "heart rate." As a result, the models presented here complement the currently accepted techniques for assessment of autonomic control of cardiovascular function. We specifically designed these techniques in order to characterize respiratory-related modulation of heart rate, but they could also be extended to model lower frequency fluctuations associated with closed loop baroreflex activity.

REFERENCES

[1] R. Berger, S. Akselrod, D. Gordon, and R. Cohen, "An efficient algorithm for spectral analysis of heart rate variability," *IEEE Trans. Biomed. Eng.*, vol. BME-33, pp. 900–904, Sept. 1986.

[2] S. Akselrod, D. Gordon, J. Madwed, N. Snidman, D. Shannon, and R. Cohen, "Hemodynamic regulation: Investigation by spectral analysis," *AJP*, vol. 249, pp. H867–H875, 1985.

[3] S. Akselrod, D. Gordon, F. Ubel, D. Shannon, A. Bargar, and R. Cohen, "Power spectrum analysis of heart rate fluctuation: A quantitative probe of beat-to-beat cardiovascular control," *Science*, vol. 213, no. 10, pp. 220–222, 1981.

[4] M. Appel, R. Berger, J. Saul, J. Smith, and R. Cohen, "Beat to beat variability in cardiovascular variables: Noise or music?," *J. Amer. Coll. Cardiol.*, vol. 14, pp. 1139–1148, 1989.

[5] A. Malliani, M. Pagani, F. Lombardi, and S. Cerutti, "Cardiovascular neural regulation explored in the frequency domain," *Circulation*, vol. 84, pp. 482–492, 1991.

[6] D. Liao, R. Barnes, L. Chambless, R. Simpson, P. Sorlie, and G. Heiss, "Age, race, and sex differences in autonomic cardiac function measured by spectral analysis of heart rate variability—The ARIC study," *Amer. J. Cariol.*, vol. 76, no. 12, pp. 906–912, 1995.

[7] G. Stanley, D. Verotta, N. Craft, R. Siegel, and J. Schwartz, "Age and autonomic effects on interrelationships between lung volume and heart rate," *Amer. J. Physiol..*, vol. 270, pp. H1833–H1840, 1996.

[8] ——, "Age effects on interrelationships between lung volume and heart rate during standing," *Amer. J. Physiol.*, vol. 273, pp. H2128–H2134, 1997.

[9] P. Grossman and M. Kollai, "Respiratory sinus arrhythmia, cardiac vagal tone, and respiration: Within- and between-individual relations," *Psychophysiology*, vol. 30, pp. 486–495, 1993.

[10] B. Pomeranz, R. Macaulay, M. Caudill, I. Kutz, D. Adam, D. Gordon, K. Kilborn, A. Barger, D. Shannon, R. Cohen, and H. Benson, "Assessment of autonomic function in humans by heart rate spectral analysis," *Amer. J. Physiol.*, vol. 248, pp. H151–H153, 1985.

[11] R. de Boer, J. Karemaker, and J. Strackee, "Comparing spectra of a series of point events particularly for heart rate variability data," *IEEE Trans. Biomed. Eng.*, vol. 31, pp. 384–387, Apr. 1984.

[12] S. Seydnejad and R. Kitney, "Real-time heart rate variability extraction using the kaiser window," *IEEE Trans. Biomed. Eng.*, vol. 44, pp. 990–1005, Oct. 1997.

[13] W. Feller, *An Introduction to Probability Theory and Its Applications*, 3rd ed. New York: Wiley, 1968, vol. 1.

[14] A. Jose, "Effect of combined sympathetic and parasympathetic blockade on heart rate and cardiac function in man," *Amer. J. Cardiol.*, vol. 18, pp. 476–478, 1966.

[15] R. de Boer, J. Karemaker, and J. Strackee, "Spectrum of a series of point events, generated by the integral pulse frequency modulation model," *Med. Biol. Eng. Comput.*, vol. 23, pp. 138–142, 1985.

[16] A. Taylor, "Autonomic control of cardiovascular function: Clinical evaluation in health and disease," *J. Clin. Pharmacol.*, vol. 34, pp. 363–374, 1994.

[17] K. Chon, T. Mullen, and R. Cohen, "A dual-input nonlinear system analysis of autonomic modulation of heart rate," *IEEE Trans. Biomed. Eng.*, vol. 43, pp. 530–542, May 1996.

[18] A. Goldberger and B. West, "Applications of nonlinear dynamics to clinical cardiology," *Ann NY Acad. Sci.*, vol. 504, pp. 195–213, 1987.

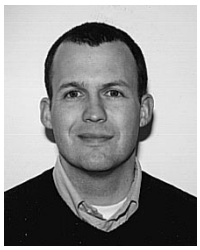

Garrett B. Stanley (S'96–A'97) graduated *summa cum laude* with a B.M.E. degree from the Georgia Institute of Technology, Atlanta, in 1992, and the M.S. and Ph.D. degrees in mechanical engineering from the University of California at Berkeley in 1995 and 1997, respectively.

From 1995–1997, he was an American Heart Association Predoctoral Fellow. From 1997–1999, he was a Postdoctoral Fellow in the Neuroscience Division of the Department of Molecular and Cell Biology at the University of California at Berkeley. He is now an Assistant Professor of Biomedical Engineering with the Division of Engineering and Applied Sciences at Harvard University, Cambridge, MA, and is an active member of the Harvard-MIT Division of Health Sciences and Technology (HST). His research interests include the modeling of biological systems, point processes, multidimensional signal processing, parameter estimation, neural coding in sensory systems, and the development of devices for recording from and stimulating the nervous system.

Kameshwar Poolla (M'00) received the B.Tech. degree from the Indian Institute of Technology, Bombay, India, in 1980, and the Ph.D. degree from the Center for Mathematical System Theory, University of Florida, Gainesville, in 1984, both in electrical engineering.

He has served on the faculty of the Department of Electrical and Computer Engineering at the University of Illinois, Urbana, from 1984 through 1991. Since then, he has been at the University of California at Berkeley where he is now serving as Professor of Mechanical Engineering. He has also held visiting appointments at Honeywell, McGill University, Montreal, PQ, Canada, and Massachusetts Institute of Technology, Cambridge, and has worked as a Field Engineer with Schlumberger AFR, Paris, France. His research interests include robust multivariable control, adaptive control, time-varying systems, system identification, process control for semiconductor manufacturing, and image processing.

Dr. Poolla received the 1984 Outstanding Dissertation Award from the University of Florida, a 1988 NSF Presidential Young Investigator Award, the 1993 Hugo Schuck Best Paper Prize (jointly with Profs. Khargonekar, Tikku, Nagpal, and Krause), the 1994 Donald P. Eckman Award, and a 1997 JSPS Fellowship.

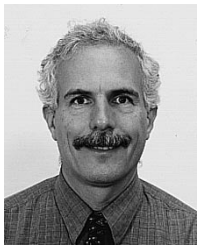

Ronald A. Siegel received the B.S. degree with honors in mathematics from the University of Oregon, Eugene, in 1975, and the M.S. and Sc.D. degrees in electrical engineering and computer science from the Massachusetts Institute of Technology, Cambridge, in 1979 and 1984, respectively.

From 1984–1998, he was on the faculty in the Departments of Biopharmaceutical Sciences and Pharmaceutical Chemistry at the University of California at San Francisco, and was a member of the Joint UCSF/UC Berkeley Bioengineering Graduate Group. In 1998, he moved to the University of Minnesota, Twin Cities, where he is Professor and Department Head of Pharmaceutics, with a faculty appointment in the Department of Biomedical Engineering. His research interests include novel drug delivery systems, bio-MEMS, modeling of transport in membranes, the physical chemistry of hydrogels, and the pharmacodynamics of drug tolerance.

Dr. Siegel received the Pfizer Young Investigator Grant Award from the American Association of Pharmaceutical Scientists (AAPS) in 1988, and the Young Investigator Award from the Controlled Release Society (CRS) in 1989. He was President of CRS during 1997–1998. In 1999 he was inducted as Fellow of the American Institute of Medical and Biological Engineering, and as Fellow of AAPS. He presently serves on the editorial boards of the *Journal of Controlled Release* and *AAPS PharmSci*.